Relationship of Carbon Crystallization to the Metal-Dusting Mechanism of Nickel

Z. Zeng* and K. Natesan

Argonne National Laboratory, Argonne, Illinois 60439

Received August 1, 2002. Revised Manuscript Received November 14, 2002

Raman scattering and X-ray diffraction (XRD) were used to study the mechanism of metal-dusting corrosion of nickel and Alloy 601. The Raman bandwidths and the relative intensities of the 1330- and 1580-cm^{-1} bands are related to the crystallinity and defect structure of coke. Both Raman and XRD analyses suggest that there is a relationship between metal dusting and the catalytic crystallization of carbon. Coke cannot crystallize well by deposition from carburizing gases at low temperature without catalytic activation because of its strong C−C bonds and high melting temperature. Participation of nickel during the coke-crystallizing process tends to improve the crystallinity of the coke. At the same time, nickel particles are liberated from metal. A decrease in free energy from highly disordered carbon to well-crystallized carbon is the driving force of metal dusting.

Introduction

In strongly carburizing gas atmospheres at carbon activities (a_C) > 1, iron-, cobalt-, or nickel-based alloys can be attacked by metal-dusting corrosion in the temperature range of 400−900 °C.[1−9] Metal-dusting corrosion occurs when carbon deposits on the surface of a metal or alloy and pits are formed, accompanied by the formation of nanosize metal carbide or pure metal particles. Metal dusting of steel components has been a problem most often in the petroleum and petrochemical industries. This form of deterioration has been studied for more than 50 years.[10]

It is believed that metal-dusting corrosion of nickel occurs in several steps.[7,8] The first steps involve carbon deposition on the surface of nickel. There are three reactions that lead to carbon deposition:

$$H_2 + CO = C + H_2O \quad a_C = K \cdot P_{H_2} \cdot P_{CO}/P_{H_2O} \qquad \text{(reaction 1)}$$

$$2CO = C + CO_2 \quad a_C = K \cdot P_{CO}{}^2/P_{CO_2} \qquad \text{(reaction 2)}$$

$$CH_4 = C + 2H_2 \quad a_C = K \cdot P_{CH_4}/P_{H_2}{}^2 \qquad \text{(reaction 3)}$$

Carbon activities calculated from the above reactions are the chemical potentials of carbon to deposit from gases. High carbon activity is the driving force for the first step. In the second step, carbon atoms dissolve and diffuse into the nickel. The second step is driven by the concentration gradient of the carbon. Graphite particles were observed to precipitate and to grow in nickel metal.[11] This process led nickel metal to separate into nanosized particles that moved away from the bulk alloy in the third step. It is necessary to study the driving force that leads carbon to precipitate and to grow in nickel metal.

Investigations into the mechanism of metal dusting have focused predominantly on defects in the metals. Defects in carbon deposition have hardly been studied, even though carbon is an integral part of the metal-dusting process. The structure of graphite is layered, with the space group $P6_3/mmc$ (see Figure 1). Carbon atoms within the layers bond strongly through sp^2 hybridization and arrange in a two-dimensional honeycomb network. The layers are stacked in a hexagonal crystalline structure and are bound together by van der Waals forces. Because the van der Waals force is weak, the C−C distance between layers is large (3.354 Å).[12] For this reason, graphite crystals readily become disordered along the *c*-axis.[13]

The structural disorder of graphite can be studied by Raman scattering.[14−17] Lattice defects in graphite break

* Corresponding author. Telephone: (630)252-9842. Fax: (630)252-3604. E-mail: zeng@anl.gov.

(1) Lefrancois, P. A.; Hoyt, W. B. *Corrosion* **1963**, *19*, 360t.
(2) Hochman, R. F. *Proceedings of the 4th International Congress on Metallic Corrosion*; Hamner, N. E., Ed.; National Association of Corrosion Engineers: Houston, TX, 1972; pp 258−263.
(3) Schueler, R. C. *Hydrocarbon Process.* **1972**, *51*, 73.
(4) Hochman, R. F. *Proceedings of the Symposium on Properties of High-Temperature Alloys with Emphasis on Environmental Effects*; Foroulis, Z. A., Pettit, F. S., Eds.; The Electrochemical Society: Princeton, 1977; pp 715−732.
(5) Nava Paz, J. C.; Grabke, H. J. *Oxidation Met.* **1992**, *39*, 437.
(6) Grabke, H. J.; Krajak, R.; Muller-Lorenz, E. M. *Werkst. Korros.* **1993**, *44*, 89.
(7) Grabke, H. J.; Krajak, R.; Muller-Lorenz, E. M.; Strauss, S. *Mater. Corros.* **1998**, *49*, 328.
(8) Grabke, H. J. *Mater. High Temp.* **2000**, *17*, 483.
(9) Maier, M.; Norton, J. F. *Mater. Corros.* **1999**, *50*, 640.
(10) Camp, E. Q.; Phillips, C.; Gross, L. *Corrosion (Houston)* **1945**, *1*, 149.
(11) Wei, Q.; Pippel, E.; Woltersdorf, J.; Strauss, S.; Grabke, H. J. *Mater. Corros.* **2000**, *51*, 652.
(12) Franklin, R. E. *Acta Crystallogr.* **1951**, *4*, 253.
(13) Krebs, H. *Fundamentals of Inorganic Crystal Chemistry*; McGraw-Hill: London, 1968; p 150.
(14) Dillon R. O.; Woollam, J. A. *Phys. Rev. B* **1984**, *29*, 3482.
(15) Tuinstra, F.; Koenig, J. L. *J. Chem. Phys.* **1970**, *53*, 1126.
(16) Nakamizo, M.; Honda, H.; Inagaki, M.; Hishiyama, Y. *Carbon* **1977**, *15*, 295.
(17) Nakamizo, M.; Honda, H.; Inagaki, M. *Carbon* **1978**, *16*, 281.

10.1021/cm020807l CCC: $25.00 © 2003 American Chemical Society
Published on Web 01/31/2003

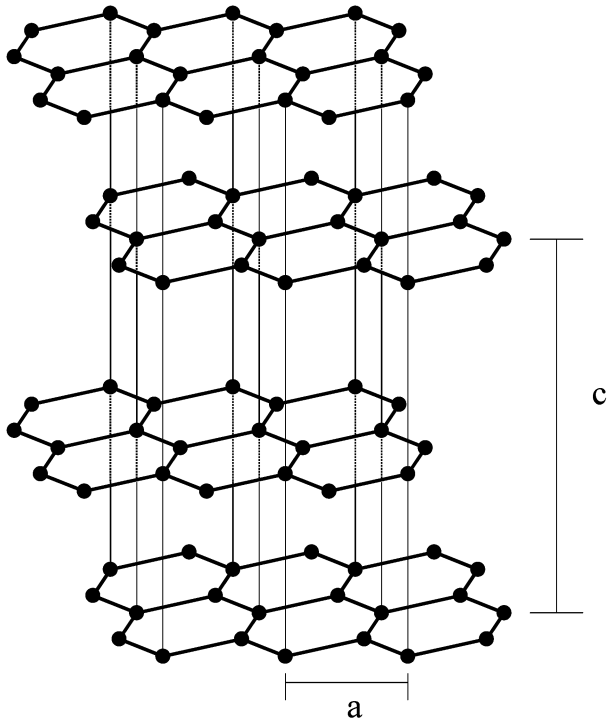

Figure 1. Structure of graphite. Carbon atoms within layers arranged in a two-dimensional honeycomb network; layers are stacked in a hexagonal crystal structure.

down the hexagonal symmetry of the graphite lattice and modify the optical selection rules for the lattice vibrational modes that are observable in Raman scattering. A single Raman line, the E_{2g} vibration mode, is theoretically expected for the hexagonal lattice of graphite and has been observed at 1575 cm^{-1} in natural graphite. In glassy carbon, the mutual orientation between the layers is random (due to the weak link between the layers). A band at 1355 cm^{-1}, observed for glassy carbon, has been assigned to a defect-activated vibrational mode that originates at the distorted hexagonal lattice of graphite near the crystal boundary. The two bands at 1355 and 1575 cm^{-1} are designated as the D (distorted) band and the G (graphite) band, respectively. It has been reported that the relative intensity ratio I_D/I_G and the relative bandwidths increase in progression from single-crystal graphite through polycrystalline graphite up to glassy carbon; hence, their values can be used as a measure of imperfection of the planes of the graphite layer.[14−17] These parameters are more defect-sensitive than are the XRD parameters that define crystalline size. Therefore, Raman spectroscopy represents a useful tool for investigating the defects in carbon structures and their relationship to metal dusting. In this paper, we present results of Raman spectroscopy measurements that are pertinent to the metal dusting of nickel and nickel-based alloys.

Experimental Section

Corrosion tests were carried out in a flowing carburizing atmosphere consisting of 72.4:8.1:17.2:2.3 (in vol %) H_2:CO_2:CO:H_2O at 593 and 704 °C. The carbon activity in the gas changes with temperature, as shown in Figure 2. Pure nickel and Alloys 601 were selected for the experiments; their compositions are listed in Table 1. The specimens were polished with 400-grit SiC

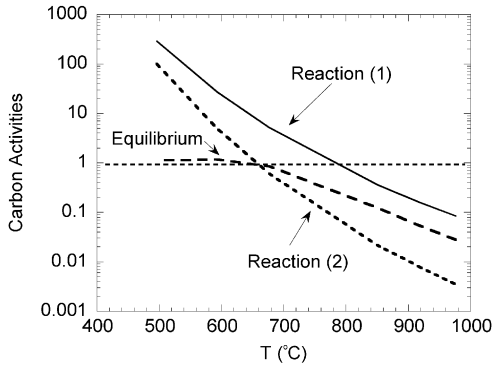

Figure 2. Carbon activity as a function of temperature for a gas mixture consisting of 72.4:8.1:17.2:2.3 (in vol %) H_2:CO_2:CO:H_2O. Curves indicated by reactions 1 and 2 indicate carbon activities calculated for reaction $CO + H_2 = C + H_2O$ and $2CO = C + CO_2$, respectively. The equilibrium curve is based on an assumption of thermodynamic equilibrium amounts of all the gas species CO, CO_2, H_2, and H_2O at each temperature.

Table 1. Composition (in wt %) of Metal and Alloys Used in Metal-Dusting Experiments

specimens	Ni	Cr	Fe	Mo	Mn	C	Si	Al
Ni	99.9							
Alloy 601	51.8	21.9	14.5	0.1	0.2	0.03	0.2	1.4

paper, and specimens were exposed in a quartz tube (38 mm in diameter) enclosed in a horizontal furnace. The nickel specimen was found to be embedded in a lot of black fine powder after exposure in the carburizing gas. This powder is conventionally called “coke”. Coke on the surface of specimens was removed by cotton tips and specimens were cleaned by ultrasonic cleaning and acetone washing. Chemical analysis showed that coke consists of 99% carbon and 1% nickel. Phases in the coke and metal samples were analyzed by X-ray powder diffraction. The microstructure of each sample was examined with a JSM-6400 scanning electron microscope. To study metallographic cross sections, the samples were electrolytically etched with 10% acetic acid at 10 V for 30 s.

Raman spectra were obtained with a Renishaw System 2000 imaging Raman microscope equipped with a He−Ne laser that delivered ∼5 mW to the specimen. The spectra were recorded in a frequency range of 190−4000 cm^{-1}, with the laser partially defocused to a diameter of ∼5 μm to avoid burning or otherwise transforming of the carbon deposits. Spectra were taken at three to six locations on a given specimen to validate that the observed surface deposits were uniform in composition.

Results and Discussion

The surface of the nickel specimen was smooth before exposure in the carburizing atmosphere (Figure 3a); the straight lines on the surface are the polishing marks made by the SiC paper. However, the nickel surface became rough (Figure 3b) after metal dusting. A tightly adhering carbon layer on the surface of the nickel could not be removed, even by ultrasonic cleaning and acetone washing. The thickness of the carbon layer was ∼40 μm, but was not uniform. Metallographic cross sections showed the separation of nickel and its subsequent incorporation in the carbon layer (Figure 4).

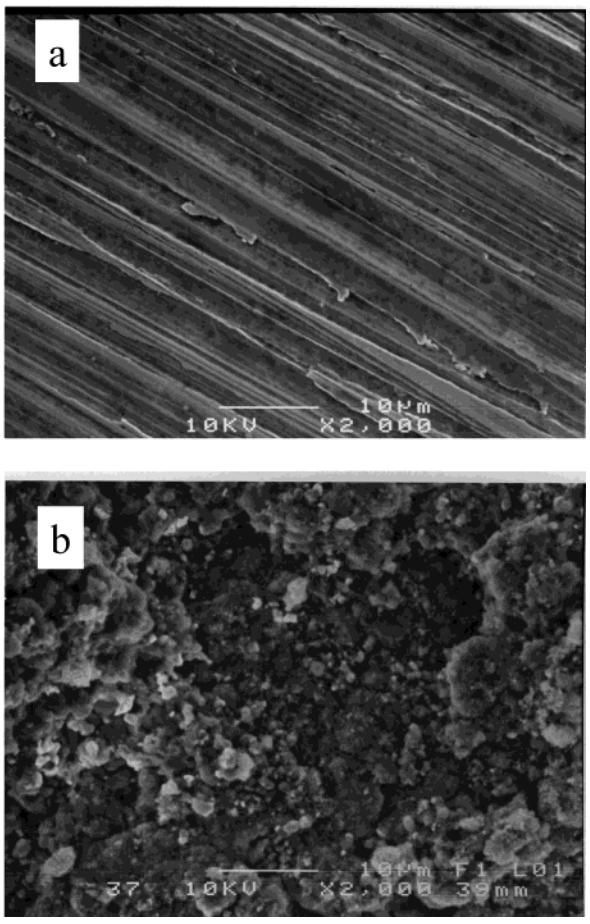

Figure 3. Surface SEM image of nickel: (a) before exposure in a carburizing atmosphere; (b) after exposure in a carburizing gas atmosphere at 593 °C for 100 h.

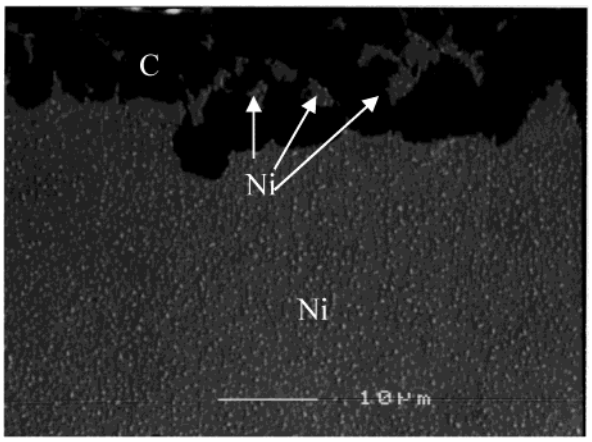

Figure 4. SEM photomicrograph of a metallographic cross section of nickel, showing a tightly bound carbon layer on the surface of nickel after ultrasonic cleaning. Nickel particles are separated into small particles and move away from the metal surface.

The surface of Alloy 601 was smooth after exposure in the carburizing atmosphere for 100 h at 593 °C (Figure 5). No metal-dusting corrosion on Alloy 601 was observed in 100 h.

The effect of Cr on metal dusting was investigated by Grabke and co-workers.[18,19] A Cr_2O_3 layer (~12-nm thick) reportedly protected the alloys from metal dusting.[19] Cr_2O_3 was observed by Raman spectroscopy on the surface of Alloys 601 tested in our study (Figure 6).

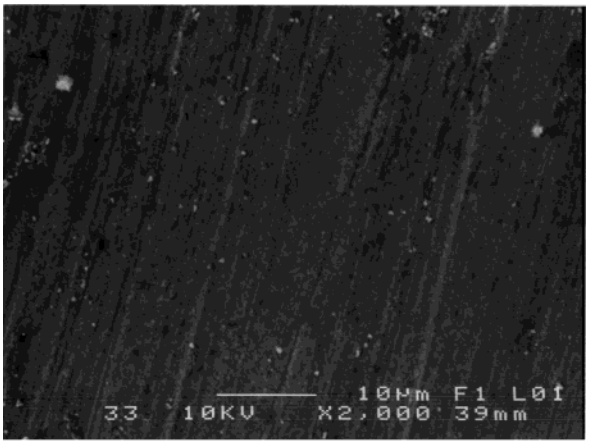

Figure 5. Surface SEM image of Alloy 601 after exposure in a carburizing gas atmosphere at 593 °C for 100 h.

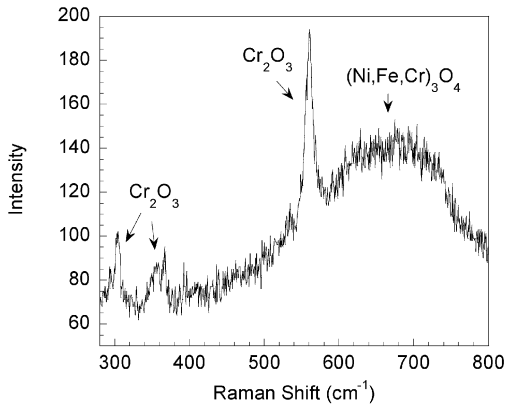

Figure 6. Raman spectrum of Alloy 601.

The 303-, 355-, and 559-cm^{-1} peaks correspond to Cr_2O_3.[20–23] The three elements iron, nickel, and chromium can also form a spinel oxide in the environment used in our study. Because the ionic radii of Fe^{2+} (0.61 Å), Cr^{3+} (0.62 Å), and Ni^{2+} (0.69 Å) are similar,[24] a random mixing of these atoms is anticipated in the spinel lattice. Therefore, the spinel oxide produces a broad band at ~680 cm^{-1}, as shown in the Raman spectra of Alloy 601.

The major phases observed in the metal-dusting product are graphite and nickel metal (Figure 7). As mentioned above, a tightly adhering carbon layer is present on the surface of the nickel. The [002] XRD peak width of this carbon layer is broader than that of well-crystallized graphite (Figure 8), a finding we interpret as indicating that the crystallinity of the carbon is inferior to that of graphite. The width of the XRD [002] of coke is even broader than that of the carbon in the adhering carbon layer; however, it is much narrower than that of carbon black, which was made by thermal

(18) Grabke, H. J.; Muller-Lorenz, E. M. *Mater. Corros.* **1998**, *49*, 317.
(19) Strauss, S.; Grabke, H. K. *Mater. Corros.* **1998**, *49*, 321.
(20) Farrow, R. L.; Benner, R. E.; Nagelberg, A. S.; Mattern, P. L. *Thin Solid Films* **1980**, *73*, 353.
(21) Thierry, D.; Persson, D.; Leygraf, C.; Delichere, D.; Joiret, S.; Pallotta, C.; Hugot-Le Goff, A. *J. Electrochem. Soc.* **1988**, *135*, 305.
(22) Maroni, V. A.; Melendres, C. A.; Kassner, T. F.; Kumar, R.; Siegel, S. *J. Nucl. Mater.* **1990**, *172*, 13.
(23) Thibeau, R. J.; Brown, C. W.; Heidersbach, R. H. *Appl. Spectrosc.* **1978**, *32*, 532.
(24) Lide, D. R. *CRC Handbook of Chemistry and Physics*, 80th ed.; CRC Press: Boca Raton, FL, 1999; pp 12−14.

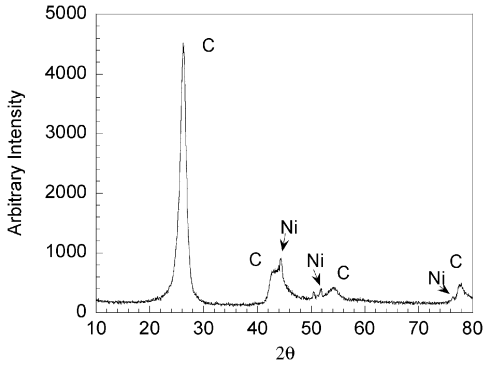

Figure 7. X-ray diffraction pattern of coke.

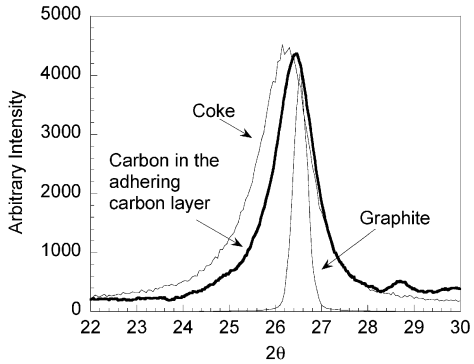

Figure 8. Peak widths of XRD 002 diffraction of graphite, coke, and carbon in the adhering carbon layer of the nickel.

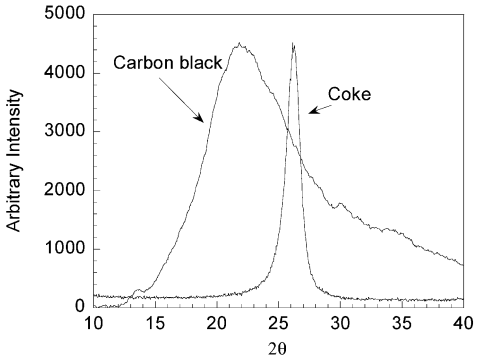

Figure 9. XRD 002 diffraction of carbon black and coke.

Table 2. Crystallite Dimension and Interlayer Plane Distance of Graphite, Coke Made at 704 and 593 °C, and Carbon Black; Δ Is the Difference between the Interlayer Plane Distance of Carbon and That of Single-Crystal Graphite (with the Interlayer Plane Distance = 3.354 Å)

carbon materials	interlayer plane distance (Å)	Δ (Å)	crystallite size (Å)	mean number of layers per particle
graphite	3.356	0.002	220	65.7
carbon made at 704 °C	3.368	0.014	106	31.5
carbon made at 593 °C	3.396	0.042	62.8	18.5
carbon black	4.026	0.672	9.9	2.5

decomposition of gasoline vapor at 704 °C (see Figure 9). Table 2 shows that the crystallite sizes of coke are much larger than that of carbon black. The crystallite sizes of cokes are also considerably larger than those reported for other carbonaceous materials made at a similar temperature.[25−27]

In Figure 9, the peak position of carbon black moves to a smaller diffraction angle, which indicates that the interlayer distances of the carbon plane are also related to the degree of disorder.[25−27] The layers are not parallel in the disorientated graphite structure. Average interlayer plane distance increases when layers are disoriented, as shown in Figure 10. The interlayer plane distance is 3.354 Å for single-crystal graphite.[12] The interlayer plane distance for coke is very close to that of the well-crystallized graphite. Franklin[12] proposed the following relationship for the proportion of disorientated layers (p) as a function of interlayer plane distance (d):

$$d = 3.44 - 0.086(1 - p^2)$$

According to this relationship, the interlayer plane distances of coke made at 593 °C (3.396 Å), seen in Table 2, is indicative of a carbon with ∼60% three-dimensional ordering. For the carbon produced by conventional treatment of carbon-containing raw materials, a heat treatment temperature >2000 °C is necessary for thermal recrystallization before this high degree of three-dimensional ordering is achieved.[12,25−28] Therefore, nickel may work as a catalyst to help the recrystallization of carbon achieve higher ordering at lower temperatures.

Raman spectra of coke, carbon black, and graphite are presented in Figure 11. The well-crystallized graphite shows a sharp band at 1580 cm^{-1}(G band) that can be assigned to the E_{2g} C−C stretching mode.[15,29,30] The first-order phonon band at 1360 cm^{-1} (D band) is not observed for well-crystallized graphite because of the $k = 0$ selection rule.[15] However, disorder in the lattice can

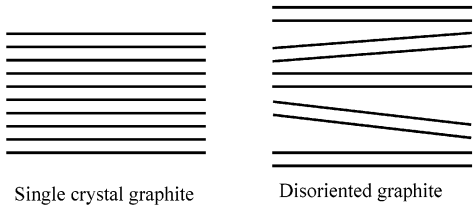

Figure 10. Average interlayer plane distance of disorientated graphite is greater than that of single-crystal graphite.

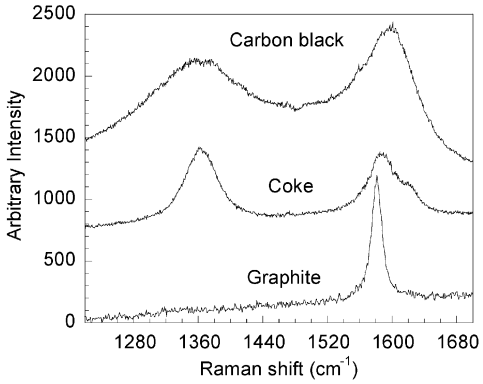

Figure 11. Raman spectra of coke, carbon black, and graphite.

(25) Blayden, H. E.; Riley, H. L.; Taylor, A. *J. Am. Chem. Soc.* **1940**, *62*, 180.
(26) Schaeffer, W. D.; Smith, W. R.; Polley, M. H. *Ind. Eng. Chem.* **1953**, *45*, 1721.
(27) Kinney, C. R. *Proceedings of the Conference on Carbon*; University of Buffalo, Buffalo, NY, 1956; p 83.
(28) Austin, A. E.; Hedden, W. A. *Ind. Eng. Chem.* **1956**, *46*, 1520.
(29) Nemanich, R. J.; Solin, S. A. *Phys. Rev. B* **1979**, *20*, 392.
(30) Al-Jishi, R. *Phys. Rev. B* **1982**, *26*, 4514.

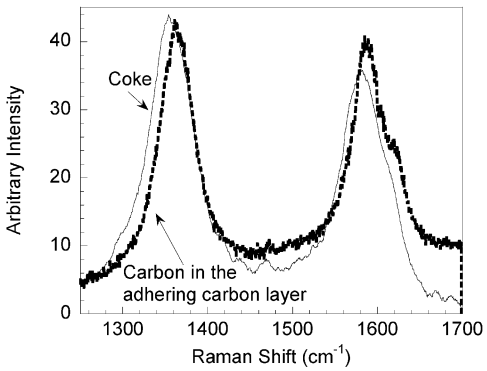

Figure 12. Raman spectra of coke and carbon in the adhering carbon layer of the nickel specimen. The relative intensity ratio I_D/I_G of coke (1.22) is larger than that of carbon on the surface of nickel (1.07), which indicates that the crystallinity of carbon on a nickel surface is better than that of coke.

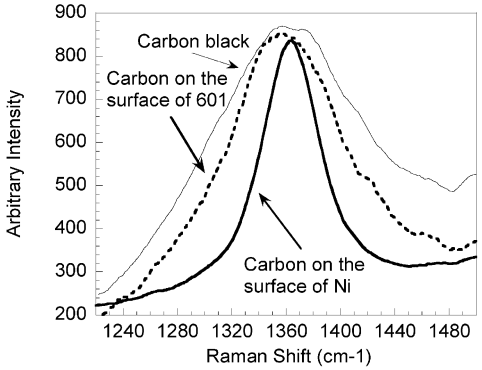

Figure 13. Raman spectra of carbon black and carbon on the surface of Alloy 601 and pure nickel.

cause a breakdown of this selection rule and thereby exhibit a band at 1360 cm^{-1} in the Raman spectra of carbon black. The highly disordered carbon exhibits very broad Raman bands, and the intensity of the 1360-cm^{-1} band increases when carbon becomes more disordered. The intensities of the D band are considered dependent on the in-plane displacements, which lead to a loss of hexagonal symmetry of the two-dimensional graphite lattice within the planes.[17] A shoulder at 1620 cm^{-1} in the cokes is also dependent on structural disorder and is, therefore, designated as the D′ band; its behavior is qualitatively similar to that of the D band.[31,32]

The widths of Raman bands for the coke from the dusting process are between those of well-crystallized graphite and carbon black, which indicates that the crystallinity of coke is better than that of carbon black, but worse than that of well-crystallized graphite. The Raman spectra in Figure 12 show that the Raman band for the carbon in the adhering carbon layer on specimen is narrower than that for coke at some distance from the surface. The relative intensity ratio I_D/I_G of coke is also larger than that of the carbon in the adhering carbon layer on specimen. These results may indicate that the crystallinity of the carbon in the adhering carbon layer on the specimen is better than that of coke, and this is consistent with XRD results.

Raman spectra indicate that a small amount of carbon is present on the surface of Alloys 601. The amount of carbon is too small to be detected by XRD; however, Raman spectra are sensitive enough to detect the carbon deposition on the oxide layers of Alloys 601. Figure 13 shows the Raman spectra of carbon on the surface of Alloy 601. The width of the Raman band of carbon on the surface of Alloy 601 is close to that of carbon black, which is deposited without catalyst. However, the width of the Raman band of the carbon in the adhering carbon layer of the nickel specimen is much narrower than that of both carbon black and the carbon on the surface of Alloy 601, which indicates that the crystallinity of the carbon in the adhering carbon layer of the nickel specimen is much better than that of the carbon on the surface of Alloy 601. The SEM image in Figure 5 shows that metal-dusting corrosion has not initiated on the surface of Alloy 601 after 100 h of exposure in a carburizing atmosphere. Carbon has not penetrated through the oxide layer on the surface of Alloy 601 in 100 h, and the oxide layer has not acted as a catalyst to aid in the catalytic crystallization of carbon. Therefore, the crystallinity of carbon on the surface of Alloy 601 is similar to that of carbon black. These results indicate that there appears to be a relationship between metal dusting and the catalytic crystallization process of the carbon because the crystallinity is good if the carbon experienced a metal-dusting process and the crystallinity is poor if the carbon has not experienced a metal-dusting process.

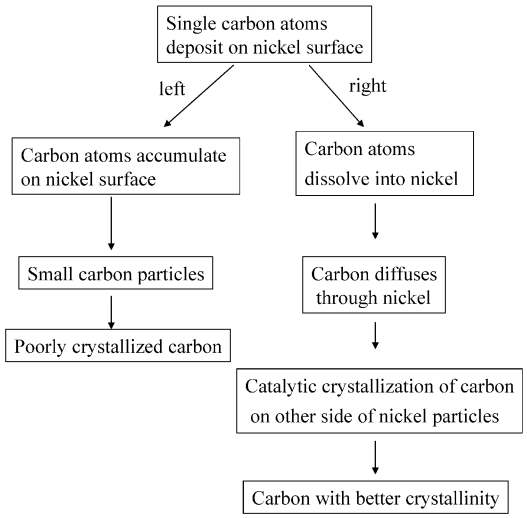

Figure 14. Proposed process for carbon crystallization after deposition from a carburizing gas. Carbon atoms accumulate on the surface and form poorly crystalline carbon particles in the left branch when the Ni lattice does not mediate the crystallization process of carbon. However, highly crystalline carbon is formed in the right branch as carbon diffuses through the nickel and the nickel lattice mediates the crystallization of carbon.

Figure 14 shows our interpretation of the crystallizing process for carbon during dusting. In the initial stage, single carbon atoms are deposited on the surface of the nickel; they then either dissolve in the nickel or accumulate to form small carbon particles. There are dangling bonds on the surface and many defects, such as vacancies and distorted bonds in the small particles. All of these surface and internal defects cause an increase in the free energy of these particles compared to that of well-crystallized graphite. At higher temper-

(31) Vidano, R.; Fischbach, D. B. *J. Am. Ceram. Soc.* **1978**, *61*, 13.
(32) Knight, D. S.; White, W. B. *J. Mater. Res.* **1989**, *4*, 385.

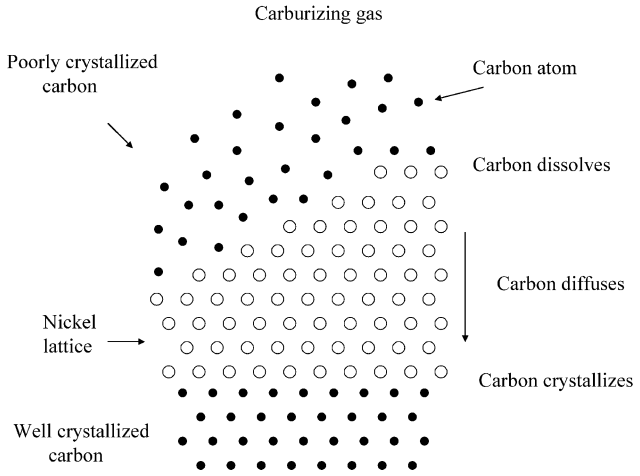

Figure 15. Disoriented carbon dissolves in and diffuses through nickel; the lattice plane of nickel gives excellent orientation to improve crystallinity of carbon.

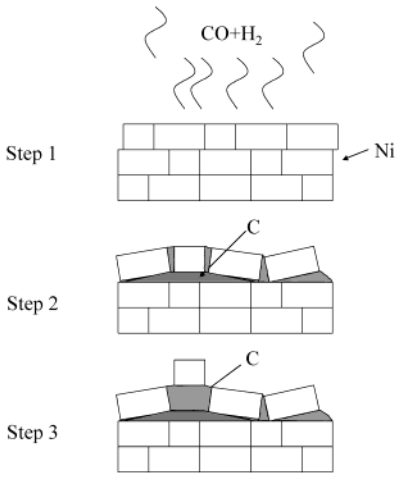

Figure 16. Carbon particles precipitate at the defects in nickel. Accumulation of carbon particles causes nickel to separate into small particles and the resultant small particles move away from the metal.

ature, where the carbon atoms have enough energy to migrate, the carbon recrystallizes from small distorted particles to large well-crystallized graphite. However, because the C−C bond is very strong (the melting temperature of carbon is 4492 °C), the recrystallization process requires a higher temperature. The rate of carbon recrystallization could be dramatically increased if nickel acts as a catalyst. When carbon dissolves in nickel, the Ni−C bond is much weaker than the C−C bond, and transport of carbon atoms is greatly facilitated. Therefore, the poorly crystallized coke can transfer through nickel and eventually achieve improved crystallinity. The free energy is then reduced by reducing the number of dangling bonds on the surface and the number of internal defects in the carbon particles.

Figure 15 shows the catalytic recrystallization process. As mentioned above, the carbon layers in the graphite structure are easily disoriented because the van der Waals forces between the layers are weak. At the upper surface of the nickel particle, there is a mismatch between the lattice planes of the nickel and graphite. This lattice mismatch retards the formation of well-crystallized graphite. If carbon grows from this nickel lattice plane, poorly crystallized carbon will form. However, carbon atoms can dissolve into and diffuse though the nickel lattice; they precipitate from a lattice plane that provides an excellent orientation for the epitaxial growth of graphite. Graphite was reported to grow with its layer plane parallel to the (111) and (110) planes of the nickel.[11] The catalytic crystallization process leads to a coke (produced during metal dusting) with a crystallite size that is much larger and an interlayer plane distance that is smaller than those of carbons made by other methods at a similar temperature.[12,25−27]

In our proposed catalytic crystallization process, carbon dissolves on the surface of the nickel and crystallizes at the defects of the bulk nickel. Because the free energy of poorly crystallized carbon is probably higher than that of well-crystallized graphite, the saturating concentrations for poorly crystallized carbon and graphite will differ. Poorly crystallized carbon should exhibit a slightly higher saturating concentration than that of graphite; hence, the saturating concentration of poorly crystallized carbon will be oversaturating for graphite; therefore, poorly crystallized carbon could dissolve in nickel and crystallize as well-crystallized graphite. The free energy difference between poorly crystallized carbon and the well-crystallized graphite drives carbon to transfer through the nickel particles and precipitate inward via the defects or grain boundary of nickel. The accumulation of carbon in an alloy causes the metal to separate, as seen in Figure 4. The metal particles finally become nanosized powder in this process until they are too small to help carbon grow to large crystals (Figure 16).

As mentioned above, the crystallinity of carbon in the adhering carbon layer of the nickel specimen is better than that of coke. This phenomenon can be explained if we assume that two types of carbon are involved in the carbon deposition and metal-dusting process. According to Figure 14, the carbon that participates during the metal-dusting process will exhibit good crystallinity. This carbon should have already diffused through the metal, whereas the carbon that is not involved in the catalytic crystallization is poorly crystallized and does not diffuse into the metal. Thus, the carbon in the adhering carbon layer of the nickel specimen should have participated in the metal-dusting process and just experienced the catalytic crystallization process. Therefore, the carbon in the adhering carbon layer of the nickel specimen exhibits better crystallinity. Coke is slightly different from the carbon in the adhering carbon layer of the nickel specimen, although their major phases are carbon. The carbon in the adhering carbon layer of the nickel specimen is “fresh” from the metal-dusting process. However, coke has been exposed to the carburizing gas for some time after the metal-dusting process. The nanosized nickel particles in coke continued to interact with carburizing gas. These particles also work as catalysts to help the deposition of carbon. However, the average size of a nickel particle in coke is only 48 nm. These nickel particles are too small to help carbon grow to large crystals. The surface areas of nanoparticles are large. Therefore, carbon has more chances to accumulate on the surface of nanosized nickel particles according to the left branch in Figure 14, and formed poorly crystallized particles. Since coke contains

these poor crystalline carbon particles, its crystallinity is worse than that of the carbon in the adhering carbon layer of the nickel specimen.

Conclusions

Raman and XRD results shed some light on the metal-dusting mechanism. Carbon on an oxide layer, which did not participate in the metal-dusting process, exhibits poor crystallinity, whereas carbon on the metal surface, which experienced the metal-dusting process, shows good crystallinity. These results indicate that the metal-dusting process involves catalytic crystallization of carbon. Nickel acts as a catalyst in this process and the catalytic crystallization causes inward transport of carbon into the nickel. The accumulation of carbon in nickel leads to separation of nickel into a fine powder and eventual degradation of the alloy by metal dusting. The difference in the free energy between poorly crystallized coke and well-crystallized graphite is the driving force for recrystallization of coke and the metal-dusting corrosion. Although the driving force is very small, it can lead to severe corrosion in the long term.

Metal dusting can be prevented or minimized by applying an appropriate oxide coating to the surface of the metal, thereby slowing the diffusion of carbon into the metal. The oxide film on the metal surface can minimize both catalytic deposition and crystallization of carbon. Chromia scales on the alloys can protect the alloys against metal-dusting corrosion.

Acknowledgment. This work was supported by the U.S. Department of Energy, Office of Industrial Technologies, under Contract W-31-109-Eng-38. The authors thank V.A. Maroni for his assistance with the Raman experiment and D. L. Rink for his assistance in conducting the metal-dusting experiments.

CM020807L